Supplementary Information

In Operando Identification of V^{4+}-Site-Dependent Nitrogen Reduction Reaction of VS_x

Rui Zhao, Xinyue Chi, Xiaoxuan Wang, Liang Zhao, Yixiang Zhou , Yuanyuan Xiong, Shuyun Yao, Shiyu Wang, Dewei Wang, Zhenzhen Fu, Zhiyu Yang, Yi-Ming Yan*

State Key Lab of Organic−Inorganic Composites, Beijing Advanced Innovation Center for Soft Matter Science and Engineering, Beijing University of Chemical Technology, Beijing, 100029, People's Republic of China

*Corresponding Author.

Email: bityanyiming@163.com

Tel (Fax): +86-10-64451521

Experimental Section

Materials

Sodium orthovanadate ($Na_3VO_4 \cdot 12H_2O$) and thioacetamide (TAA, CH_3CSNH_2) were commercially available from Shanghai Chemical Reagent Co. Ltd. Ammonium metavanadate (NH_4VO_3) were from Shanghai Macklin Biochemical Co.Ltd. Hydrazine hydrate ($N_2H_4 \cdot H_2O$) and ethanol (C_2H_5OH) were purchased from Beijing Tongguang Fine Chemical Co., Ltd. Hydrochloric acid (HCl), salicylic acid ($C_7H_6O_3$, ≥99.7%), ammonium chloride (NH_4Cl, 99.998%), p-dimethylaminobenzaldehyde (p-$C_9H_{11}NO$, 99%), trisodium sodium citrate dehydrate ($C_6H_5Na_3O_7 \cdot 2H_2O$, 99%), sodium nitroferricyanide dihydrate ($C_5FeN_6Na_2O \cdot 2H_2O$, 99%), sodium hypochlorite solution (NaClO, available chlorine 6-10%) were purchased from Beijing Chemical Corp. Nafion (5 wt%) was purchased from Sigma-Aldrich Chemical Reagent Co., Ltd. All the chemicals were used without further purification. Ultrapure Smart-S15 water (18.2 MΩ) was used in all experiments.

Preparation of VS$_{2-x}$ and VS$_2$. 3 mmol $Na_3VO_4 \cdot 12H_2O$ and 15 mmol TAA powders were dissolved in 30 mL DI water in a glass jar, which was then stirred for 1 h to form a homogeneous solution and transferred to a 50 mL Teflon-lined autoclave. The autoclave was sealed and heated at 180 °C for 2 h. After it was cooled down to room temperature, a black precipitate was collected by centrifugation and washed several times with DI water and absolute ethanol, VS$_{2-x}$ were produced. Then, the experiments proceed again with changing V source to NH_4VO_3, VS$_2$ were obtained.

Preparation of VS$_{2-x}$ and VS$_2$ electrode. VS$_{2-x}$ was prepared as following: First, 5 mg of VS$_{2-x}$ catalyst and 20 μL of Nafion solution (5 wt%) were dispersed in 980 μL mixed solution contain

ethanol and H_2O (V : V = 2 : 1) by 1h sonication to form a homogeneous ink. Then 20 μL of the VS_{2-x} ink was loaded on a carbon paper (1 cm × 1 cm) and dried. The VS_2 was prepared by following the same method.

Characterizations. The X-ray diffraction (XRD, Rigaku D/MAX 2550) equipped with Cu Kα radiation (λ = 1.54178 Å) by scanning from 2θ = 5 to 90º was used to analyze crystalline structures. A field emission scanning electron microscopy (SEM, JEOL JSM-6700F) was used to analyze the surface morphology of samples. The high-resolution TEM, TEM images were recorded on a Zeiss Libra 200FE TEM operated at 200 kV. The chemical compositions of the materials were characterized by X-ray photoelectron spectroscopy (XPS, Physical Electronics 5400 ESCA). The surface area of the samples was estimated by method of Brunauer-Emmett-Teller (BET) was made by application of the Barrett-Joyner-Halenda (BJH) method to the adsorption data. The Raman spectrum was recorded on a HORIBA Raman microscope with a laser wavelength of 532 nm (LabRAM Aramis, HORIBA Jobin Yvon S.A.S, France) for surface characterization. The absorbance data of spectrophotometer were measured on UV-8000S UV-Vis spectrophotometer (Shanhai Metash Instruments Co., Ltd). The X-ray absorption spectra (XAS) including X-ray absorption near-edge structure (XANES) and extended X-ray absorption fine structure (EXAFS)of the samples at V K-edge (5477 eV were collected at the Singapore Synchrotron Light Source (SSLS) center, where a pair of channel-cut Si (111) crystals was used in the monochromator. The V K-edge XANES data were recorded in a transmission mode. V foil were used as references. The storage ring was working at the energy of 2.5 GeV with average electron current of below 200 mA. The acquired EXAFS data were extracted and processed according to the standard procedures using the ATHENA module implemented in the FEFIT software packages. The k^3-weighted

Fourier transform (FT) of x(k) in R space was obtained over the range of 0-14.0 Å^{-1} by applying a Besse window finction.

Electrochemical Measurements. Before NRR measures, the Nafion membrane was pretreated by heating in H_2O_2 solution (3 wt%), 0.5 M H_2SO_4, and ultrapure water at 80°C for 2 h, respectively. Electrochemical measurements N_2 reduction experiments were carried out in a typical H-type electrolytic cell, which was separated by the Nafion 117 membrane. The electrochemical experiments were performed with a CHI 760E electrochemical analyzer (CH Instruments, Inc., Shanghai, China) using a standard three-electrode system including prepared VS$_{2-x}$/CP electrode, platinum gauze electrode and Ag/AgCl electrode serving as the working electrode, counter electrode and reference electrode, respectively. The potentials reported in this work were converted to RHE scale via calibration with the following equation: E (vs. RHE) = E (vs. Ag/AgCl) + 0.197 + 0.0591 × pH. For N_2 reduction experiments, the 0.1 M HCl electrolyte was purged with N_2 for 30 mins before the measurement. N_2 electrochemical reduction was conducted in N_2-saturated 0.1 M HCl solution. Before the controlled potential electrolysis for hours, N_2 was purged into HCl solution for at least 30 mins to remove residual air.

The LSV curves were conducted with the CHI 760e electrochemical workstation with scan rate of 10 mV s^{-1}. In 0.1 M HCl, the corresponding LSV curve was measured by purging 30 mins with Ar, and then purging N_2 for 30 minutes to measure the corresponding LSV curve. The impedance spectroscopy (EIS) measurements were tested by AC voltage with 5 mV amplitude in the frequency range of 10^5 Hz to 10^{-2} Hz under applied voltage ranging from 0 to 0.7 V vs. RHE. The potential step chronoamperometry measurement were measured at the potentials from the open-circuit voltage to the best reduction overpotential.

Determination of NH$_3$. Concentration of produced NH$_3$ was determined by the indophenol blue method. In detail, 2 mL post-tested solution was removed from the cathodic chamber, and then added into 2 mL 1.0 M NaOH solution containing C$_7$H$_6$O$_3$ and C$_6$H$_5$Na$_3$O$_7$·2H$_2$O (5 wt%), then added 1 mL NaClO (0.05 M) and 0.2 mL Na$_2$[Fe(NO)(CN)$_5$]·2H$_2$O (1 wt%) aqueous solution in turn. After standing at room temperature for 2 h, the UV-Vis absorption spectrum was measured. The concentration-absorbance curves were calibrated using standard NH$_4$Cl solution (0.1 M HCl as mother solution) with a serious of concentrations. Typically, 100 μg mL^{-1} NH$_4$Cl solution was prepared and diluted to 2 μg mL^{-1}. Then, 0.0, 0.1, 0.2, 0.4, 0.6, 0.8, 1.0 and 1.2 mL NH4Cl solutions with concentration of 2 μg mL^{-1} were poured into test tubes and separately diluted to 2 mL with 0.1 M HCl and the resulting concentrations of NH$_4$Cl in the solutions are 0.0, 0.1, 0.2, 0.4, 0.6, 0.8, 1.0 and 1.2 μg mL^{-1}. The concentration of indophenol blue was determined using the absorbance at a wavelength of 655 nm. The fitting curve (y = 0.4202x + 0.0844, R^2 = 0.9949) shows good linear relation of absorbance value with NH$_4$Cl concentration by three times independent calibrations.

Determination of N$_2$H$_4$. The hydrazine present in the electrolyte was estimated via the method of Watt and Chrisp. A mixture of p-C$_9$H$_{11}$NO (5.99 g), HCI (concentrated, 30 mL) and C$_2$H$_5$OH (300 mL) was used as a color reagent. In detail, 2 mL electrolyte was removed from the electrochemical reaction vessel and added into 2 mL above prepared color reagent and stirring 15 mins at room temperature. The absorbance of the resulting solution was measured at 455 nm. The concentration absorbance curves were calibrated using standard N$_2$H$_4$·H$_2$O solution with a series of concentrations. The fitting curve (y = 1.0548x + 0.0102, R^2 = 0.9998) shows good linear relation of absorbance value with N$_2$H$_4$ concentration.

Calculations of NH₃ formation rate and Faradaic efficiency (FE). The rate of formation of NH₃ was calculated using the following equation:

$$V\left(\mu g\ h^{-1}mg_{cat}^{-1}\right) = \frac{17 \times c_{NH_4Cl} \times V}{53.5 \times t \times m_{cat}}.$$

The FE was calculated according to the following equation:

$$FE = \frac{3 \times F \times c_{NH_4Cl} \times V \times 10^{-6}}{53.5 \times Q} \times 100\%.$$

where c_{NH_4Cl} (µg mL⁻¹) is the measured concentration of NH₄Cl; V (mL) is the volume of electrolyte (in our work 30 mL); t (s) is the reduction reaction time; m_{cat} (mg) is the mass loading of catalyst on CP; F is Faraday constant (96500 C mol⁻¹); Q (C) is the quantity of applied charge/electricity.

Calculation details. Spin-polarized density functional theory (DFT) simulations were performed to calculate the adsorption of N₂ molecule using the Vienna ab initio simulation package (VASP).[1,2] The Perdew-Burke-Ernzerhof (PBE) functional within the framework of generalized gradient approximation (GGA) was applied to describe the exchange−correlation interactions.[3,4] DFT-D2 method was adopted to consider the van der Waals (vdW) interaction.[5] For structural optimization, the Brillouin zone was sampled by 3×3×1 k-points for plane-wave basis, together with an energy cutoff of 500 eV. All the atoms were allowed to relax until the residue forces on each atom were less than 0.02 eV/Å. The convergence criterions were set to 10-5 eV for total energy. In order to avoid interactions between periodic images, a vacuum space of 10 Å was applied to all calculations. The formation Gibbs free energy (ΔG) of the NRR intermediates is calculated as:

$$\Delta G = \Delta E_{ad} + \Delta ZPE - T\Delta S$$

Where ΔE_{ad} is the adsorption energy of NRR intermediates, ΔZPE is the change of zero-point energies, ΔZPE is the zero point energy difference, T is the temperature (T = 298.15K), and ΔS is the entropy changes. The entropy of gas molecules is taken from standard values.

Supplementary Figures
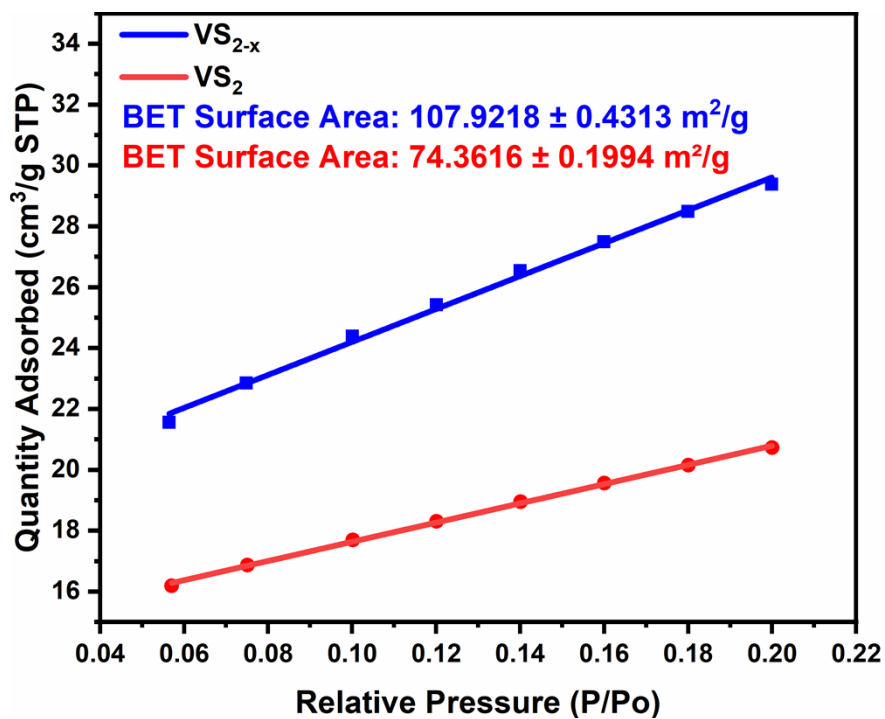
Fig S1. The BET measurement of VS_{2-x} (blue) and VS_2 (red).
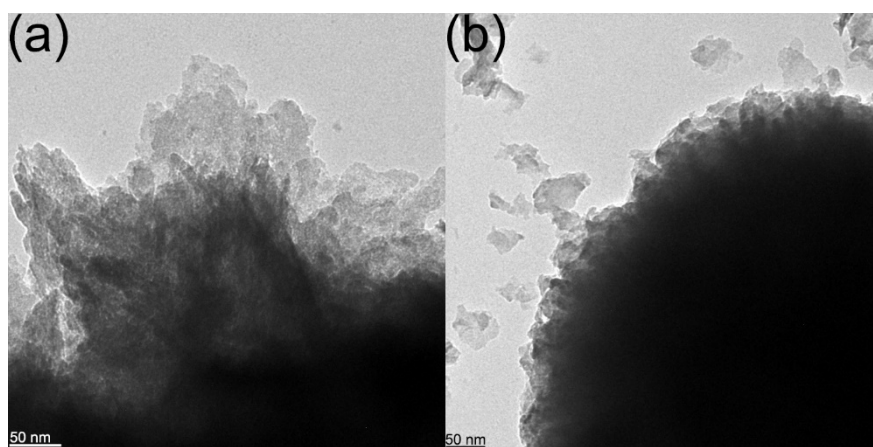
Fig S2. (a) (b)The 50 nm scale TEM image of VS_{2-x} and the 50 nm scale TEM image of VS_2.
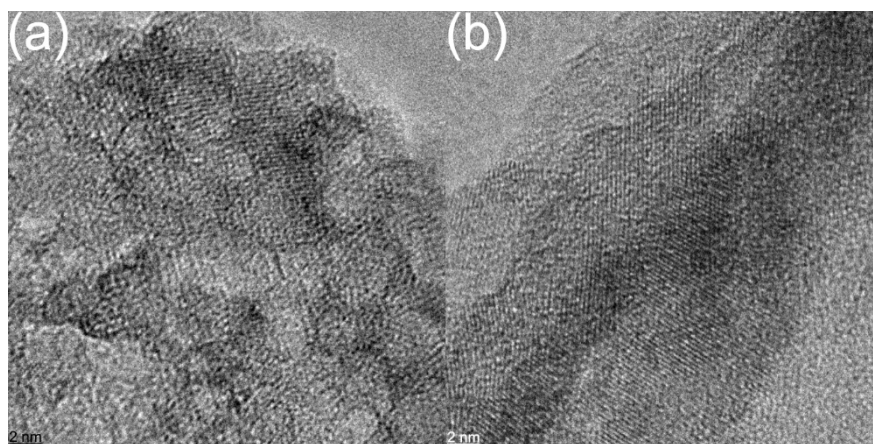
Fig S3. (a) (b)The 2 nm scale HRTEM image of VS_{2-x} and the 2 nm scale HRTEM image of VS_2.
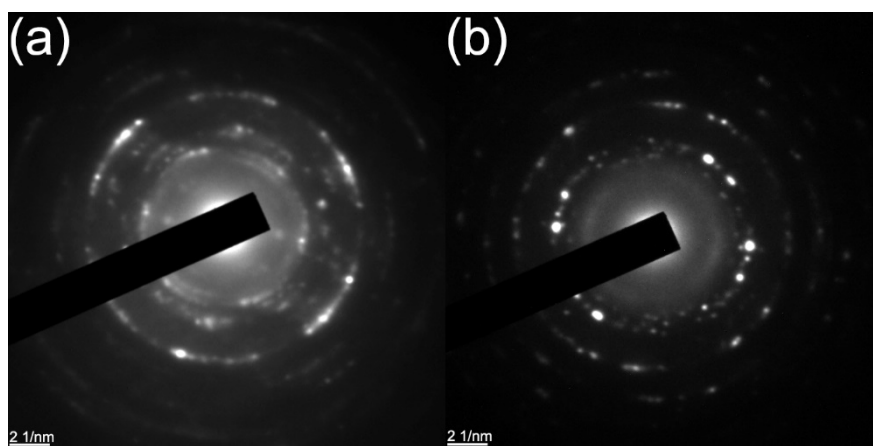
Fig. S4. (a) (b)The SAED images of VS_{2-x} and VS_2.
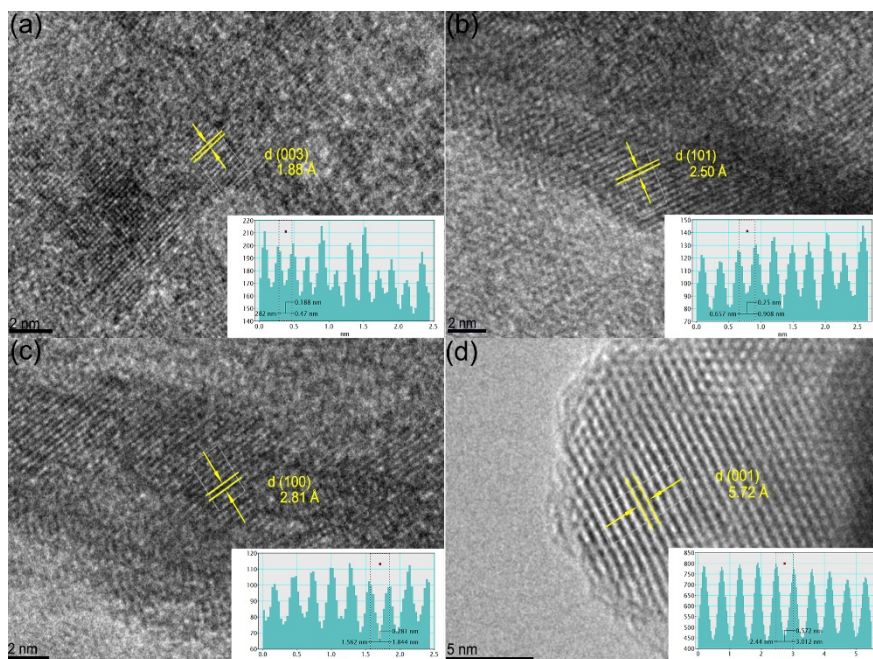
Fig S5. The HRTEM images of VS_{2-x} (a, b and c) and VS_2 (d).
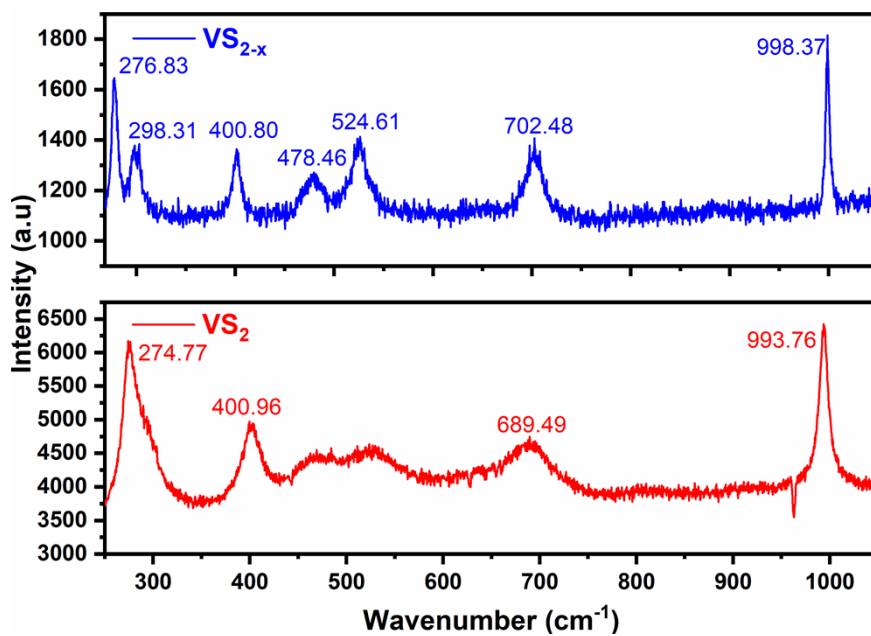
Fig S6. Raman spectra of VS_{2-x} (blue) and VS_2 (red).
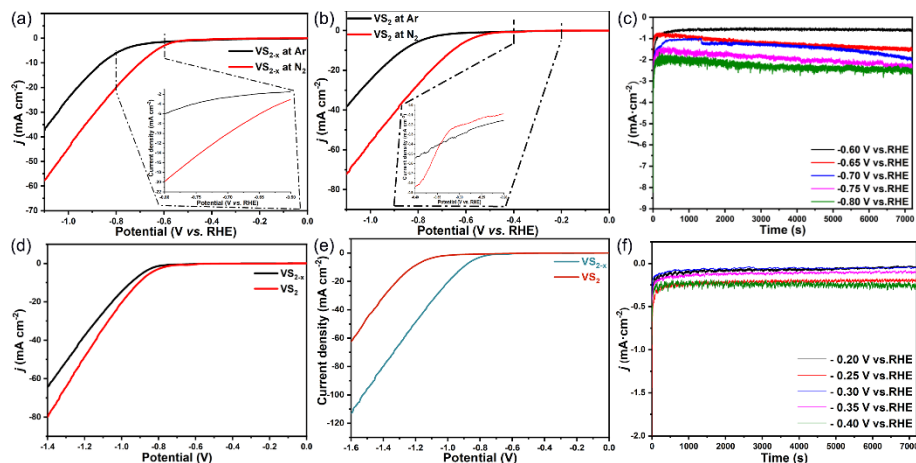
Fig S7. (a) LSV curves of VS_{2-x} at different atmospheres include N_2 (red) and Ar (black), (b) LSV curves of VS_2 at different atmospheres include N_2 (red) and Ar (black), (c) Chronoamperometry curves of VS_{2-x} at considered potentials, (d) LSV curves of VS_{2-x} (black) and VS_2 (red) at N_2 atmosphere, (e) HER performance of VS_{2-x} (blue) and VS_2 (red), (f) Chronoamperometry curves of VS_2 at considered potentials.
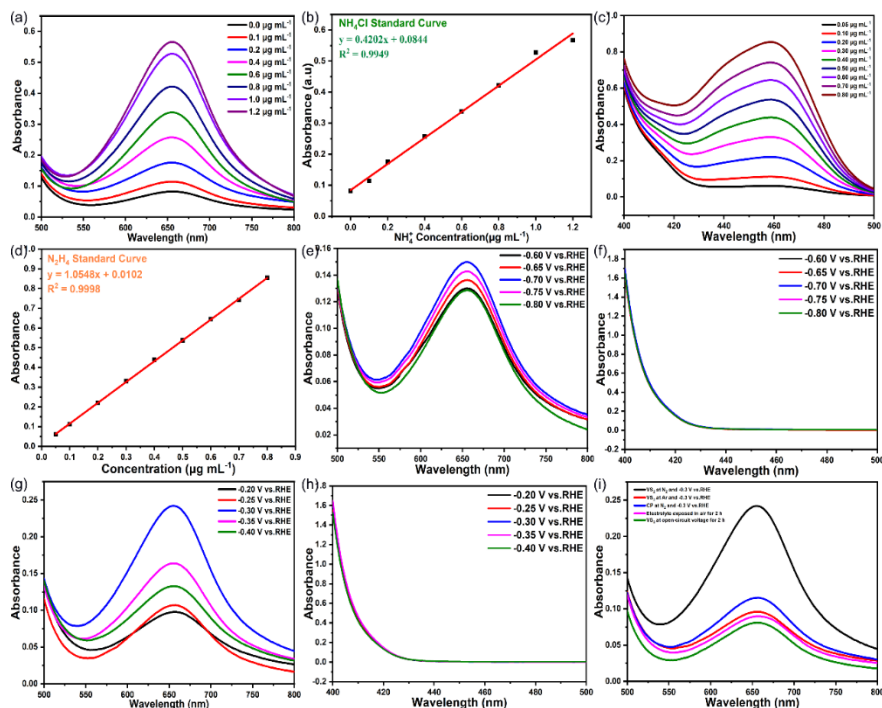
Fig S8. NH_4Cl of (a) the Uv-vis spectrum curves at a series of standard solutions, (b) the corresponding standard curve; N_2H_4 of (c) the Uv-vis spectrum curves at a series of standard solutions, (d) the corresponding standard curve; VS_{2-x} of (e) the NH_4Cl Uv-vis spectrum curves at given potentials, (f) the N_2H_4 Uv-vis spectrum curves at given potentials; VS_2 of (g) the NH_4Cl Uv-vis spectrum curves at corresponding potentials, (h) N_2H_4 Uv-vis spectrum curves at corresponding potentials; (i) the NH_4Cl Uv-vis spectrum curves of the NH_3 sources tests.

11
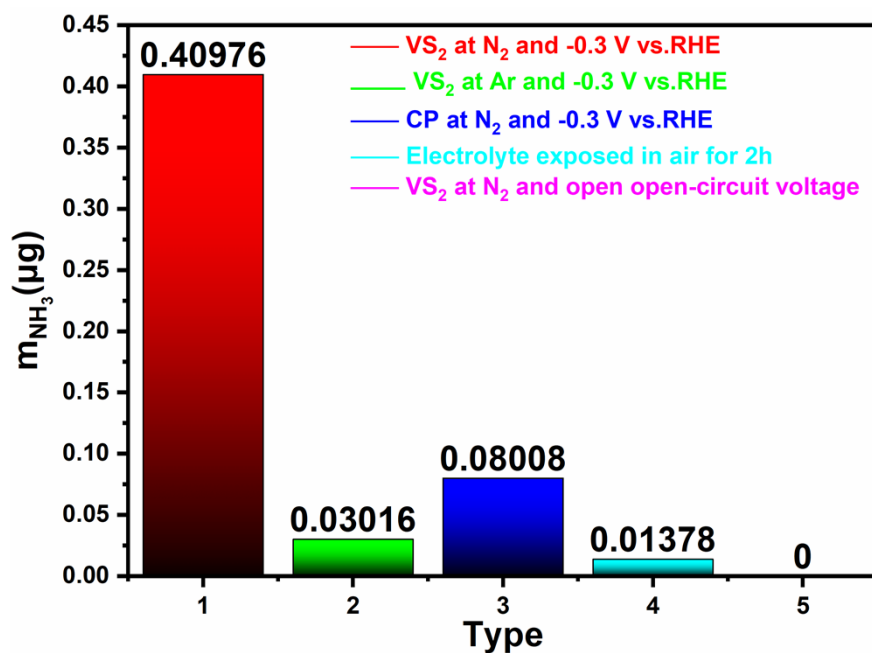
Fig S9. Ammonia sources tests of VS$_2$.
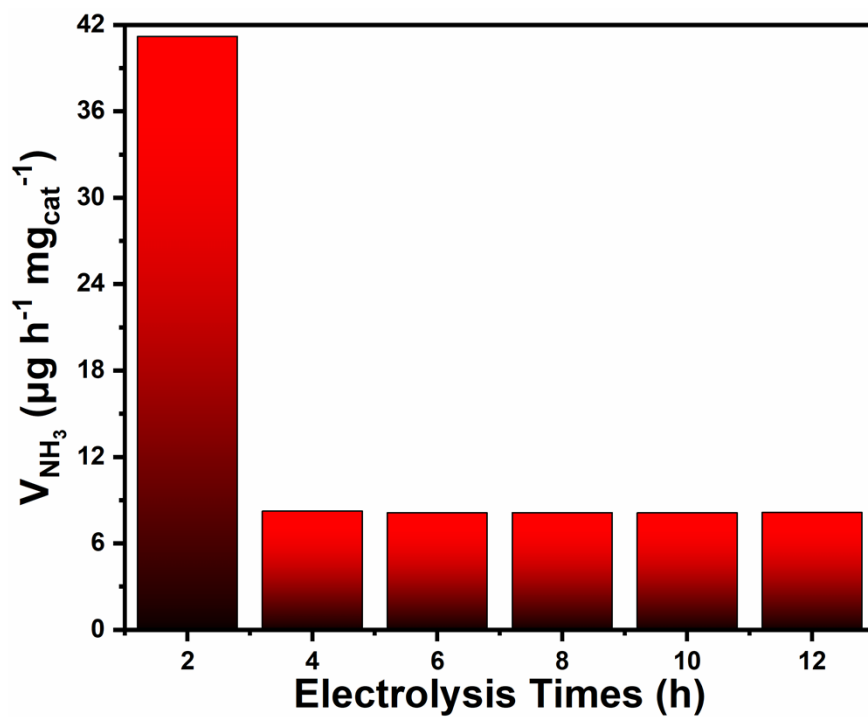
Fig S10. The cycling stability of VS$_2$, the experiments were all tested at -0.3 V Vs. RHE.
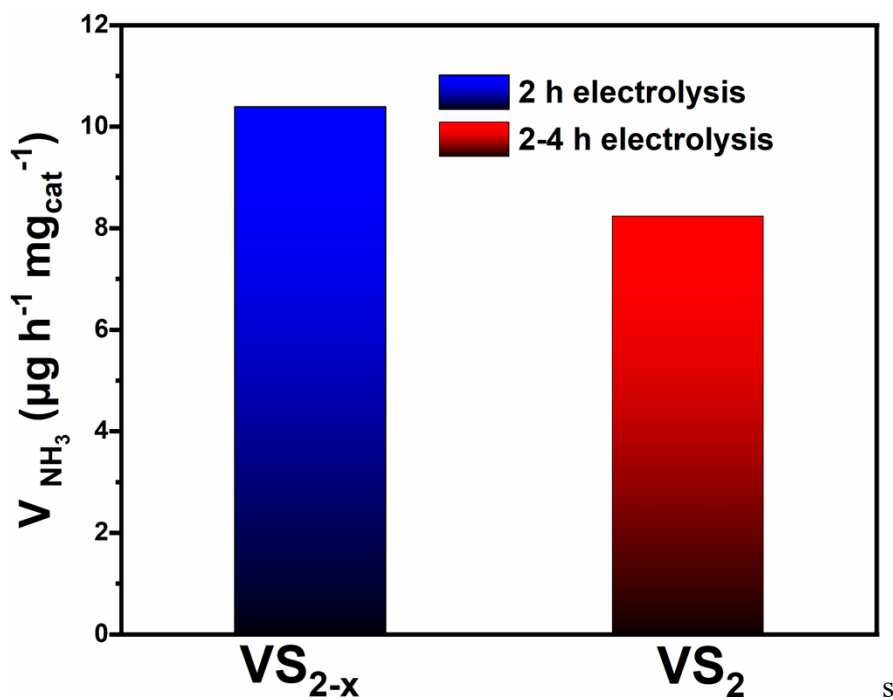
Fig S11. the Absorbance of VS$_{2-x}$ after 2 h electrolysis (blue) and VS$_2$ during 2-4 h electrolysis (red) at the same potential of -0.3 V vs. RHE.
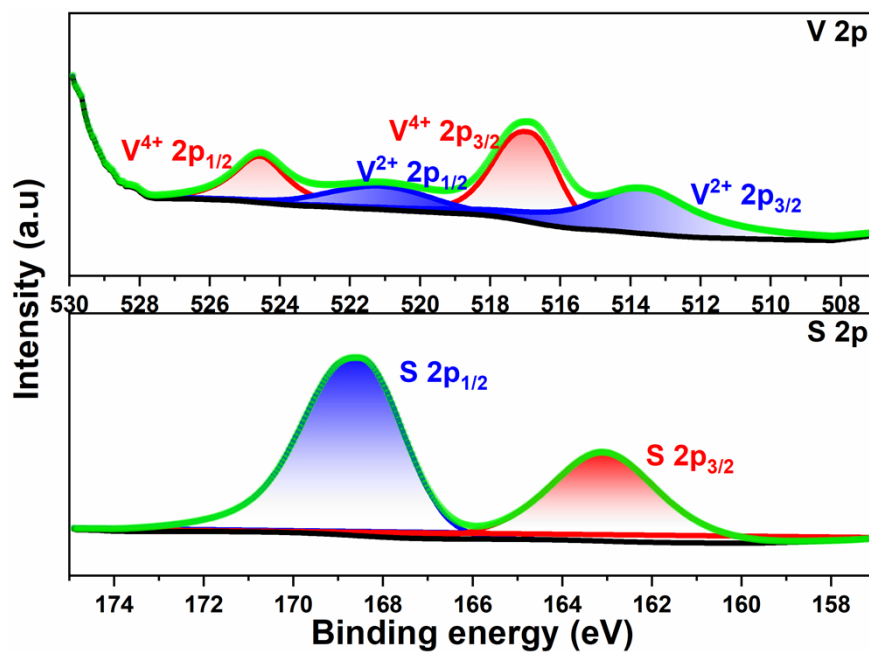
Fig S12. The XPS pattern after 2 h electrolysis for VS$_2$.
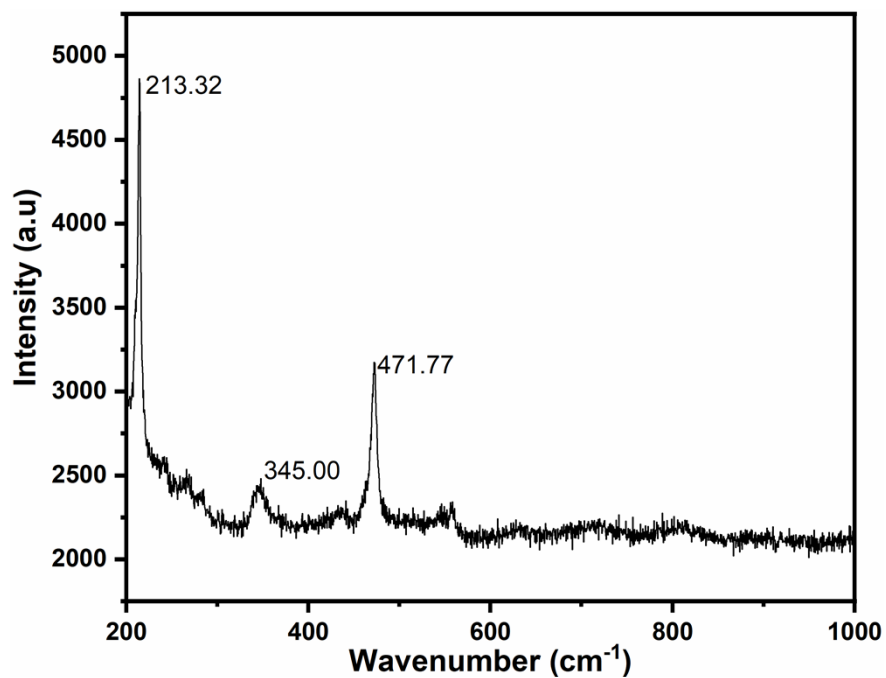
Fig S13. the Raman spectra of VS_2 in the in-situ electrochemical cell before the electrolysis.
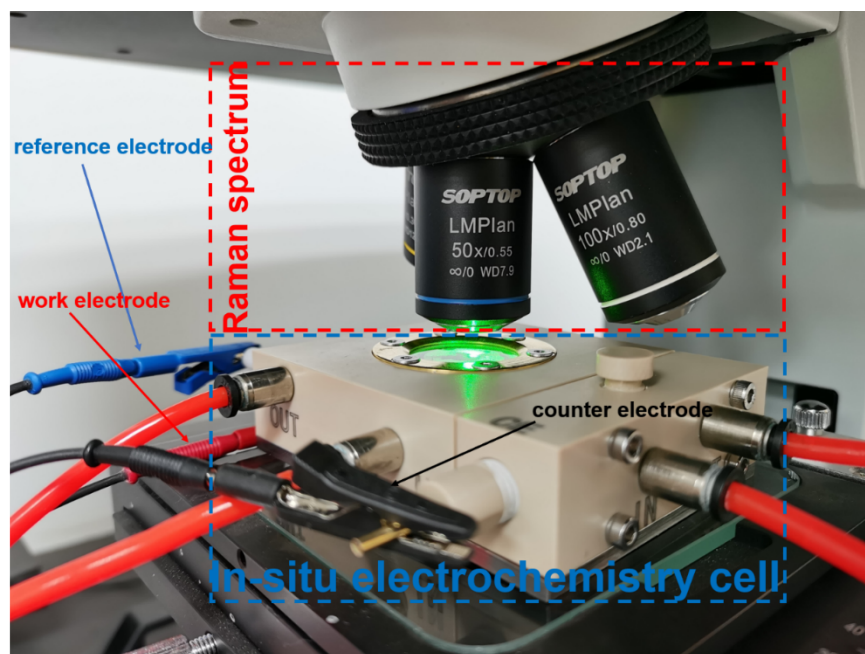
Fig S14. The in-site Raman spectrum.
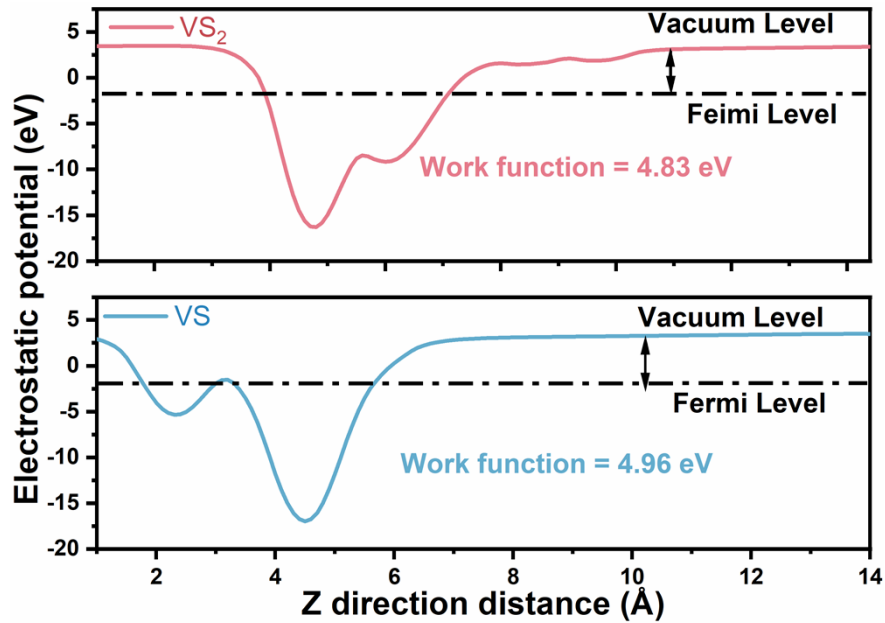
Fig S15. Work function of VS (blue) and VS$_2$ (red).
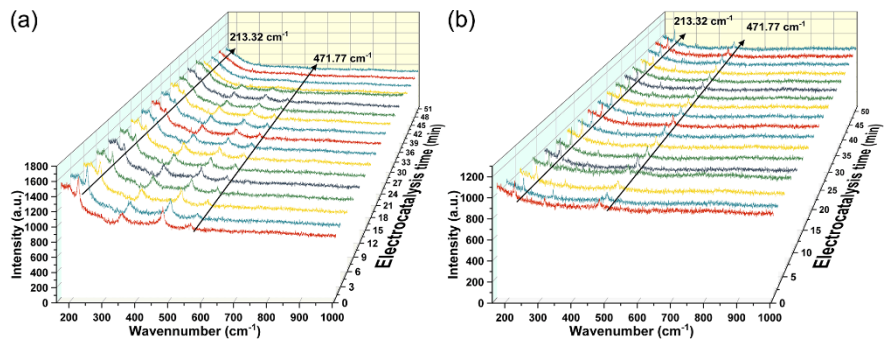
Fig S16. (a) The in-situ Raman test results for VS$_{2-x}$, (b) The in-situ Raman test results for VS$_2$ in electrochemical cell without electrolysis.
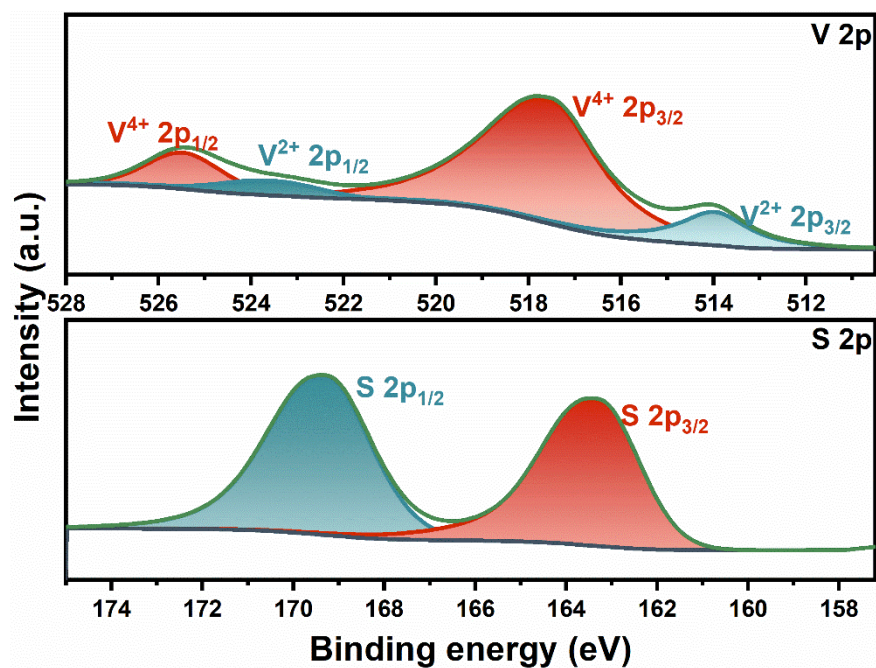
Fig S17. The XPS pattern after 2 h electrolysis for VS$_{2-x}$.
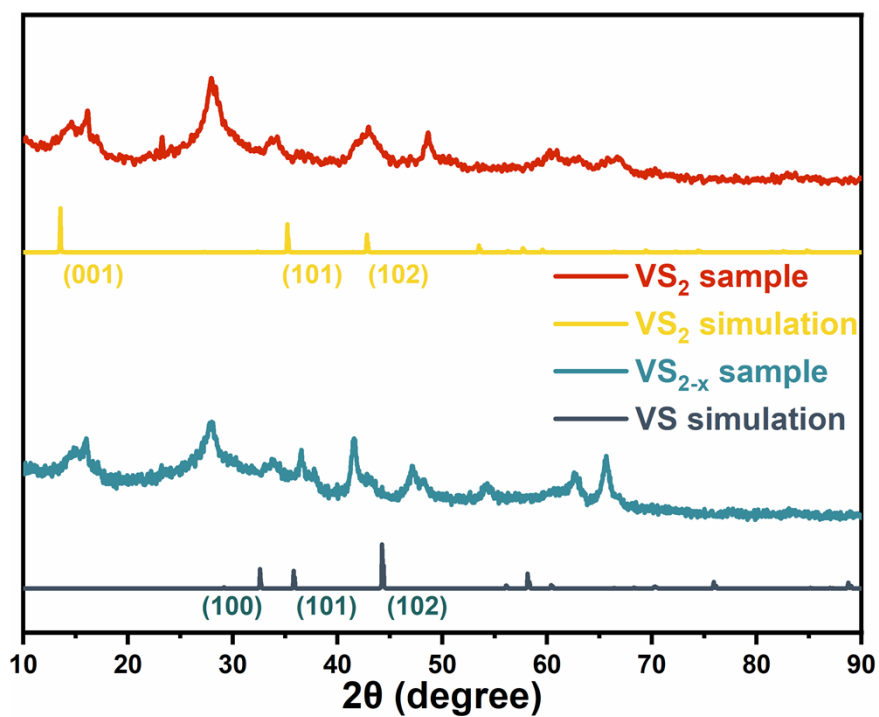
Fig S18. The simulation results for VS (PDF#02-1242) (yellow) and VS$_2$ (36-1139) (grey).
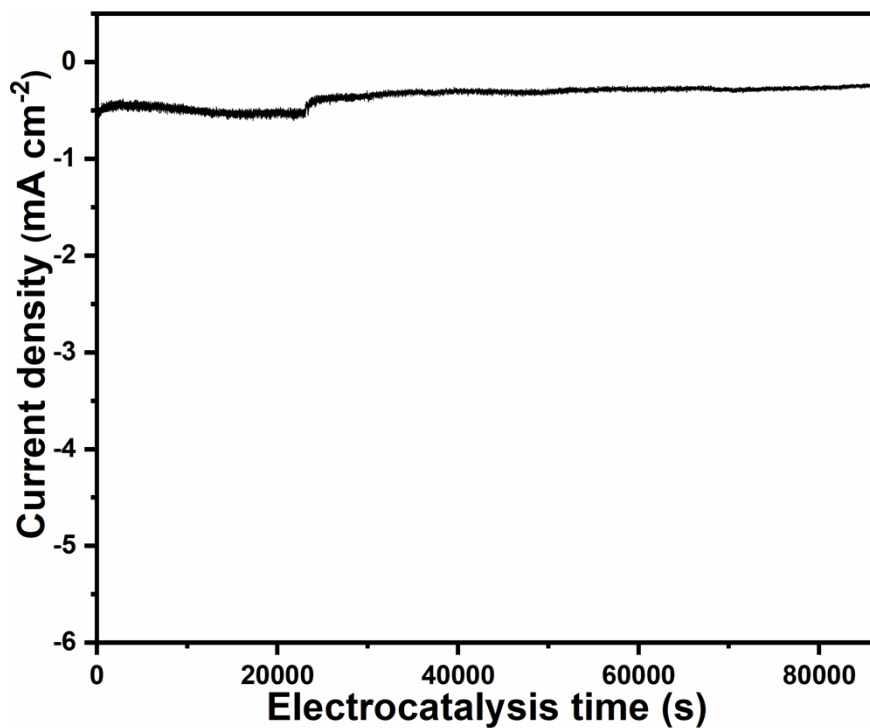
Fig S19. The long-term stability i-t test curve of VS$_2$.
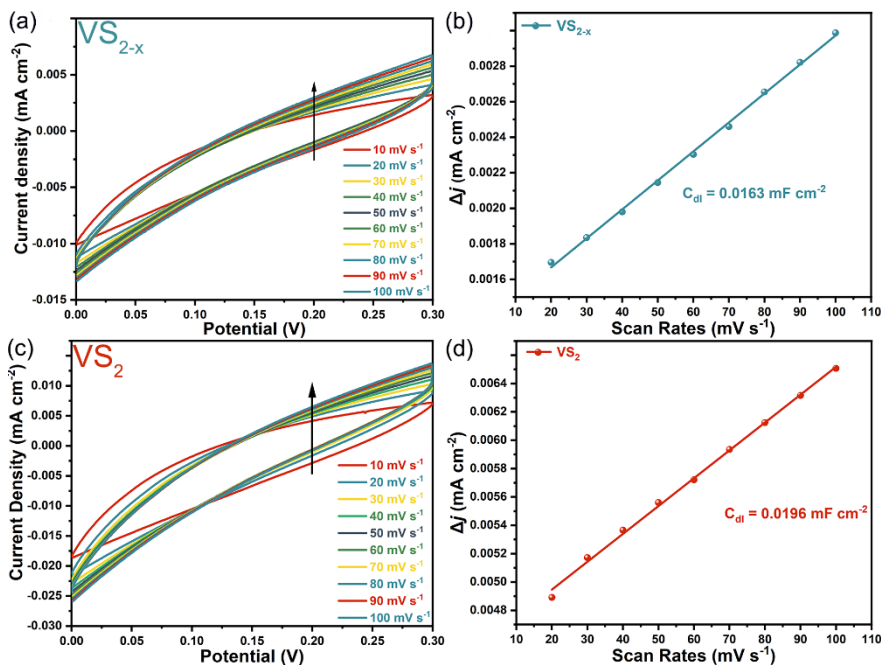
Fig S20. (a) The CV test of VS$_{2-x}$ with a series of different scan rates range from 10 to 100 mV s^{-1} (step: 10 mV s^{-1}), (b) The Cdl results for VS$_{2-x}$, (c) The CV test of VS$_2$ with a series of different scan rates range from 10 to 100 mV s^{-1} (step: 10 mV s^{-1}), (d) The Cdl results for VS$_2$.

Table S1. Performance comparisons of ENRR electrocatalysts in aqueous solutions under ambient condition.

Catalyst	Electrolyte	NH$_3$ yield rate	FE/%	Reference
VS$_2$	0.1 M HCl	41.21 µg mg$_{cat}^{-1}$ h^{-1}	35.52	This work
MoO$_2$@MoO$_3$	0.05 M H$_2$SO$_4$	60.9 µg mg^{-1} h^{-1}	23.80	6
Zn^{1}N–C	0.1 M KOH	16.1 µg mg^{-1} h^{-1}	11.80	7
NbTiO$_4$@NCNR-1	0.01 M HCl	58.13 ± 8 µg mg^{-1} h^{-1}	10.40 ± 1.40%	8
Ag-Cu$_{NS}$/CP	0.1 M Na$_2$SO$_4$	61.5 µg mg$_{cat}^{-1}$ h^{-1}	20.90	9
np-MoSe$_2$	0.1 M Na$_2$SO$_4$	30.83 µg mg^{-1} h^{-1}	37.82	10
NC/Bi SAs/TiN/CC	0.1 M Na$_2$SO$_4$	76.15 µg mg$_{cat}^{-1}$ h^{-1}	24.60	11
Pt-HEX	0.1 M KOH	26.4 µg cm^{-2} h^{-1}	1.80	12
FeMoPPc	0.1 M KOH	36.33 µg mg$_{cat}^{-1}$ h^{-1}	20.62	13
BNQDs@Nb$_2$CT$_x$	0.5 M LiClO$_4$	66.3 µg mg^{-1} h^{-1}	16.70	14
NiSb	0.1 M HCl	56.9 µg mg^{-1} h^{-1}	48.00	15
TiO$_2$	0.05 M H$_2$SO$_4$ with 20 wt% PEG400	1.07 µmol cm^{-2} h^{-1}	32.13	16
Sb/Nb$_2$CT$_x$	0.5 M LiClO$_4$	49.8 µg mg^{-1} h^{-1}	27.3	17
1T''' MoS$_2$	0.1 M Na$_2$SO$_4$	9.09 µg mg^{-1} h^{-1}	13.6	18
MXene/TiFeO$_x$-700	0.05 M H$_2$SO$_4$	21.9 µg mg^{-1} h^{-1}	25.44	19
MoS$_2$/NC-900	0.1 M Na$_2$SO$_4$	36.1 µg mg$_{cat}^{-1}$ h^{-1}	15.2	20

CoFe$_2$O$_4$	0.1 M Na$_2$SO$_4$	30.97 μg mg$_{cat}^{-1}$ h^{-1}	11.65	21
Cu$_{2-x}$S/MoS$_2$	0.1 M Na$_2$SO$_4$	22.1 μg mg$_{cat}^{-1}$ h^{-1}	6.06	22
Bi@C-900	0.1 M Na$_2$SO$_4$	4.22 ± 0.33 μg mg$_{cat}^{-1}$ h^{-1}	15.10 ± 0.43	23
Pd$_3$Bi	0.05 M H$_2$SO$_4$	59.05 ± 2.27 μg mg$_{cat}^{-1}$ h^{-1}	21.52 ± 0.71	24

References

1. Kresse, G. and Furthmüller, J. *Comput. Mater. Sci.* 1996, **6**, 15−50.

2. Kresse, G. and Furthmüller, J. *Phys. Rev. B* 1996, **54**, 11169−11186.

3. Perdew, J. P.; Burke, K. and Ernzerhof, M. *Phys. Rev. Lett.* 1996, **77**, 3865−3868.

4. Kresse, G.; Joubert, D. *Phys. Rev. B* 1999, **59**, 1758-1775.

5. Blöchl, P. E. *Phys. Rev. B* 1994, **50**, 17953−17979.

6. H. Tan, Q. Ji, C. Wang, H. Duan, Y. Kong, Y. Wang, S. Feng, L. Lv, F. Hu, W. Zhang, W. Chu, Z. Sun and W. Yan, *Nano Res.*, 2021, DOI: 10.1007/s12274-021-3934-6.

7. Y. Kong, Y. Li, X. Sang, B. Yang, Z. Li, S. Zheng, Q. Zhang, S. Yao, X. Yang, L. Lei, S. Zhou, G. Wu and Y. Hou, *Adv. Mater.*, 2022, **34**, e2103548.

8. D. K. Yesudoss, H. Chun, B. Han and S. Shanmugam, *Appl. Catal. B*, 2022, **304**.

9. Y. Qu, T. Dai, Y. Cui, Y. Zhang, Z. Wang and Q. Jiang, *Chem. Eng. J.*, 2022, **433**, 133752.

10. D. Chen, M. Luo, S. Ning, J. Lan, W. Peng, Y. R. Lu, T. S. Chan and Y. Tan, *Small*, 2022, **18**, e2104043.

11. Z. Xi, K. Shi, X. Xu, P. Jing, B. Liu, R. Gao and J. Zhang, *Adv. Sci.*, 2022, **9**, 2104245.

12. C. Du, C. Qiu, Z. Fang, P. Li, Y. Gao, J. Wang and W. Chen, *Nano Energy*, 2022, **92**.

13. Y. Wang, W. Cheng, P. Yuan, G. Yang, S. Mu, J. Liang, H. Xia, K. Guo, M. Liu, S. Zhao, G. Qu, B. A. Lu, Y. Hu, J. Hu and J. N. Zhang, *Adv. Sci.*, 2021, **8**, e2102915.

14. K. Chu, X. Li, Q. Li, Y. Guo and H. Zhang, *Small*, 2021, **17**, e2102363.

15. G. Fan, W. Xu, J. Li, J. L. Chen, M. Yu, Y. Ni, S. Zhu, X. C. Su and F. Cheng, *Adv. Mater.*, 2021, **33**, e2101126.

16. Y. Guo, J. Gu, R. Zhang, S. Zhang, Z. Li, Y. Zhao, Z. Huang, J. Fan, Z. Chen and C. Zhi, *Advanced Energy Materials*, 2021, **11**.

17. X. Li, Y. Luo, Q. Li, Y. Guo and K. Chu, *Journal of Materials Chemistry A*, 2021, **9**, 15955-15962.

18. G. Lin, Q. Ju, X. Guo, W. Zhao, S. Adimi, J. Ye, Q. Bi, J. Wang, M. Yang and F. Huang, *Adv. Mater.*, 2021, **33**, e2007509.

19. Y. Guo, T. Wang, Q. Yang, X. Li, H. Li, Y. Wang, T. Jiao, Z. Huang, B. Dong, W. Zhang, J. Fan and C. Zhi, *ACS Nano*, 2020, **14**, 9089-9097.

20. X.-W. Lv, X.-L. Liu, Y.-J. Suo, Y.-P. Liu and Z.-Y. Yuan, *ACS Nano*, 2021, **15**, 12109-12118.

21. C. Wang, L.-L. Gu, S.-Y. Qiu, J. Gao, Y.-C. Zhang, K.-X. Wang, J.-J. Zou, P.-J. Zuo and X.-D. Zhu, *Appl. Catal. B*, 2021, **297**.

22. T. Jiang, L. Li, L. Li, Y. Liu, D. Zhang, D. Zhang, H. Li, B. Mao and W. Shi, *Chem. Eng. J.*, 2021, **426**.

23. Y. Wan, H. Zhou, M. Zheng, Z. H. Huang, F. Kang, J. Li and R. Lv, *Adv. Funct. Mater.*, 2021, **31**.

24. X. Wang, M. Luo, J. Lan, M. Peng and Y. Tan, *Adv. Mater.*, 2021, **33**, e2007733.